CHEMISTRY OF MATERIALS

COMMUNICATION

pubs.acs.org/cm

Synthesis and Comparison of the Magnetic Properties of Iron Sulfide Spinel and Iron Oxide Spinel Nanocrystals

John H. L. Beal,[†] Sujay Prabakar,[†] Nicola Gaston,[‡] Geok B. Teh,[§] Pablo G. Etchegoin,[†] Grant Williams,[‡] and Richard D. Tilley*[,†]

[†]School of Chemical & Physical Sciences and the MacDiarmid Institute of Advanced Materials & Nanotechnology, Victoria University of Wellington, P.O. Box 600, Wellington, New Zealand

[‡]Industrial Research Ltd and the MacDiarmid Institute, P.O. Box 31 310, Lower Hutt, New Zealand

[§]School of Arts and Science, Tunku Abdul Rahman College, P.O. Box 10979, 50932 Kuala Lumpur, Malaysia

Supporting Information

KEYWORDS: iron sulfide, iron oxide, nanocrystals, magnetic nanoparticles, spinel, magnetite,

The iron−sulfur system contains a number of phases possessing complex and interesting chemical, magnetic and electronic properties,[1,2] including Fe_3S_4, which is isostructural to the iron oxide spinel phase Fe_3O_4. Submicrometer Fe_3S_4 nanoparticles occur in nature as magnetosomes in magnetotactic bacteria,[3] and as inclusions in geological sediments, where they are significant contributors to chemical remnant magnetization (CRM).[4,5] Yet the synthesis of monodisperse Fe_3S_4 nanocrystals and the study of their magnetic properties have received relatively little attention compared to well-researched Fe and Fe_3O_4 nanocrystals.[6−8] This is mainly due to the relatively narrow range of thermal stability of Fe_3S_4 and the tendency for formation of mixtures of iron sulfide phases,[11] making the synthesis of phase-pure, crystalline, monodisperse Fe_3S_4 nanocrystals highly challenging.

Nanocrystalline Fe_3S_4 has been synthesized using hydrothermal methods,[9,10] and monodisperse 2.5−4.5 nm[11] and 16 nm[12] Fe_3S_4 nanocrystals have been synthesized successfully from single-source precursors; these latter syntheses involve the preparation of specific single-source iron sulfide-precursors and can involve extended reaction times. In contrast, the approach reported here uses the simple and rapid in situ sulfidization of the decomposition product of iron(II) acetylacetonate ($Fe(acac)_2$), to form Fe_3S_4 nanocrystals with diameters <10 nm. The flexibility of this method allows the synthesis of monodisperse Fe_3O_4 nanocrystals of the same average diameter as Fe_3S_4 to enable a direct comparison of magnetic properties. Fe_3O_4 nanocrystals are made by omitting the sulfidization step and allowing atmospheric oxidation during work-up. The magnetic properties of the Fe_3S_4 and Fe_3O_4 nanocrystals were studied experimentally, and the results were compared to theoretical models to understand the origin of differences in temperature and size dependent magnetic properties.

In a typical synthesis of Fe_3S_4 nanocrystals, $Fe(acac)_2$ (0.30 g, 1.2 mmol) and hexadecylamine (HDA) (15 g) were flushed with N_2. The HDA was then melted and degassed by bubbling through N_2 for 30 min, and the solution was heated to 300 °C for 2 h. Elemental sulfur (1.5 equiv) dissolved in oleylamine (OA) (0.06 g, 1.8 mmol sulfur in 3.6 cm^3 OA) was injected rapidly, and the reaction mixture was then immediately cooled to room temperature with a water bath. The nanocrystals were isolated by diluting the reaction mixture with an equal volume of hot ethanol, and separating the precipitate by centrifugation. Repeated cycles of sonication of the precipitate in hot ethanol followed by centrifugation removed HDA residues. Size selective purification was used to concentrate the smaller size fraction (see the Supporting Information for full experimental details).

A low-magnification TEM image of the Fe_3S_4 nanocrystals is shown in Figure 1A, which have an average diameter of 6.5 ± 0.5 nm (inset). SAED and XRD patterns of the samples are shown in Figure SI-1A in the Supporting Information and Figure 1C, respectively; and were both indexed to the characteristic inverse spinel structure of Fe_3S_4. A comparison of the XRD pattern with the literature pattern of $Fe_{1-x}S$ (see Figure SI-2 in the Supporting Information) shows that the as-synthesized Fe_3S_4 nanocrystals contain no substantial impurities. EDS analysis (see Figure SI-3A in the Supporting Information) found an Fe:S ratio of 1:1.36, close to the expected ratio of 1:1.33 for stoichiometric Fe_3S_4. Figure 1B shows a typical low magnification TEM image of monodisperse Fe_3O_4 nanocrystals with an average diameter of 6.0 ± 0.2 nm. SAED and XRD patterns of the nanocrystals are shown in Figure SI-1B in the Supporting Information and Figure 1C, respectively; and were indexed to Fe_3O_4. EDS analysis (see Figure SI-3B in the Supporting Information) found an Fe:O ratio of 1:1.34, as expected for stoichiometric Fe_3O_4.

Magnetic measurements were conducted on both samples (see the Supporting Information for details), with ZFC/FC plots for Fe_3S_4 and Fe_3O_4 nanocrystals shown in Figure 2. The ZFC/FC plot of the Fe_3S_4 nanocrystals (Figure 2A) has an inflection centered at 50 K, indicating a transition to superparamagnetism above this temperature (i.e., average $T_B \approx 50$ K), however the ZFC and FC plots do not coincide, indicating the retention of some degree of magnetic irreversibility, which may be due to a small amount of high coercivity $Fe_{1-x}S$ impurity. A slight decrease in the susceptibility of the FC curve below the blocking temperature indicates some degree of antiferromagnetic order. In contrast, the ZFC/FC plot of the

Received: January 27, 2011
Revised: April 7, 2011
Published: April 21, 2011

dx.doi.org/10.1021/cm2002868 | *Chem. Mater.* 2011, 23, 2514–2517

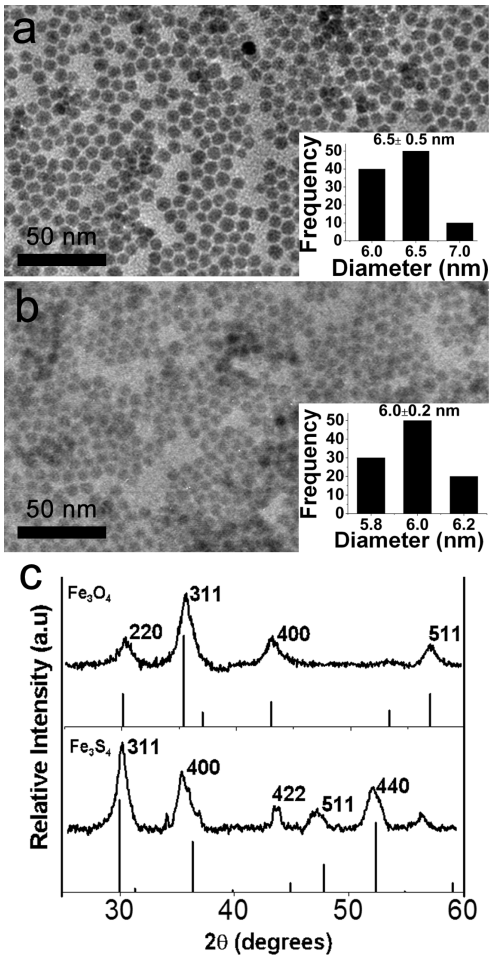

Figure 1. TEM images of (a) Fe_3S_4 nanocrystals, (b) Fe_3O_4 nanocrystals. Insets show histogram of nanocrystal diameters. (c) XRD patterns of Fe_3O_4 and Fe_3S_4 nanocrystals and reference patterns.

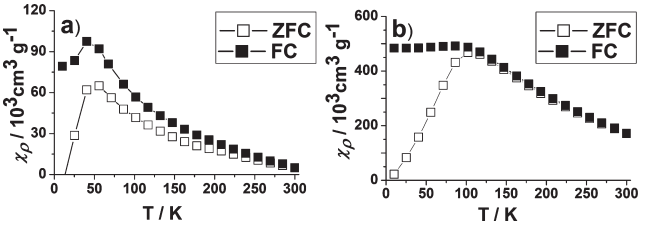

Figure 2. ZFC/FC plots of (a) Fe_3S_4 and (b) Fe_3O_4 nanocrystals.

Fe_3O_4 nanocrystals Figure 2B displays a distinct transition at 100 K, with the ZFC and FC plots coinciding above this temperature, and no decrease in the susceptibility of the FC curve below the blocking temperature. The shape of the FC curves of the samples indicates a degree of interparticle interaction, which can lead to an increase of T_B, when compared to a noninteracting ensemble.[13]

Field loops for both samples at 10 and 300 K are shown in Figure 3. At 10 K, the field loop for Fe_3S_4 nanocrystals Figure 3A displays very low coercivity at low-field, but is very slightly wasp-waisted at moderate fields (with $H_c \approx 140$ Oe), indicating the presence of a high coercivity component either due to larger Fe_3S_4 nanocrystals or $Fe_{1-x}S$ impurity. At both temperatures the field loop for the Fe_3S_4 nanocrystals has a slanted appearance at high field,

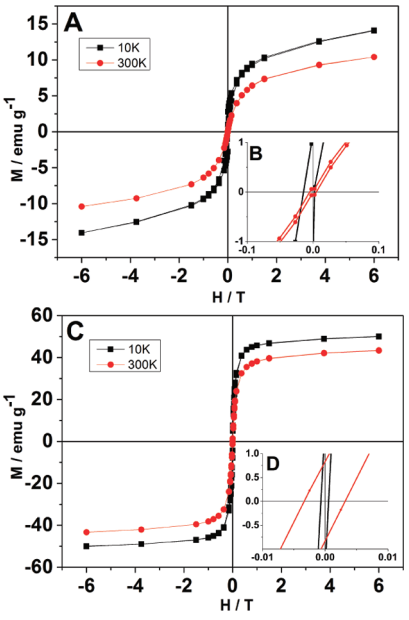

Figure 3. Field loops of (a) Fe_3S_4 nanocrystals at 10 K and 300K, (b) inset showing hysteretic behavior. (c) Fe_3O_4 nanocrystals at 10 K and 300K and (d) inset showing hysteretic behavior.

indicating the presence of a paramagnetic component, which is not saturated at 6 T. Because of this, the saturation magnetization, M_s, for the Fe_3S_4 nanocrystals can only be approximated as 12 and 9 emu g^{-1} at 10 and 300 K, respectively. The room temperature saturation magnetization of 9 emu g^{-1} measured for 6.5 nm nanocrystals is larger than that seen for 2.5−4.5 nm Fe_3S_4 nanocrystals (1.5−2.0 emu g^{-1}),[11] but is significantly smaller than that reported recently for 30 nm nanoplates (26-31 emu g^{-1}),[14] indicating that the saturation magnetization has a strong size dependence. Field loops for Fe_3O_4 nanocrystals (Figure 3C, D) display little coercivity (≤25 Oe) at either 10 or 300 K. At both temperatures, the field loops have square profiles and saturate fully at high field. The Fe_3O_4 nanocrystals have M_s values of 50 and 43 emu g^{-1} at 10 and 300 K, respectively.

To explore the differences in magnetic properties of the two phases, calculations were performed of the energetics and magnetic properties of the bulk spinels, as a function of lattice parameter. DFT calculations use PAW potentials[15] and the PW91[16] functional as implemented in VASP5.2,[17] unless otherwise stated. For the sake of comparison, the LDA[18] functional was also used.

Particle size is known to affect magnetic susceptibility through a number of mechanisms, including alteration of lattice parameter.[19] The variation in magnetic moment with respect to lattice parameter was calculated for Fe_3S_4 and Fe_3O_4, and is shown in the Supporting Information-Figure SI-4. Observed saturation magnetizations for both bulk and nanocrystalline Fe_3S_4 and Fe_3O_4, and calculated magnetizations for the energy-minimized models are tabulated in Table 1. The calculated (DFT-PW91) magnetization of the Fe_3O_4 spinel is 112 emu g^{-1}, which is slightly higher than the experimental value for bulk Fe_3O_4 of 91 emu g^{-1}.[20] The calculated lattice parameter for the bulk is 8.43 Å, in good agreement with the experimental value of 8.40 Å. The experimental value of 43 emu g^{-1} obtained in this work for the saturation magnetization of 6 nm nanocrystals at 300 K is consistent with previous literature results of 40−42 emu g^{-1} for 7−10 nm Fe_3O_4 nanocrystals.[19,20] The factor of 2 reductions

dx.doi.org/10.1021/cm2002868 |Chem. Mater. 2011, 23, 2514–2517

Table 1. Magnetic Properties of Fe_3S_4 and Fe_3O_4 Nanocrystals

		M_s (emu g^{-1})		T (K)
bulk Fe_3S_4	calcd	43		0
	obsd	38[21]		4
bulk Fe_3O_4	calcd	112		0
	obsd	91[20]		4
		M_s (emu g^{-1})		
		10 K	300 K	T_B (K)
Fe_3S_4 nanocrystals	obsd	12	9	~50
Fe_3O_4 nanocrystals	obsd	50	43	100

in the magnetization of nanocrystalline Fe_3O_4 relative to the bulk is attributable to the particle size through a combination of surface effects which contribute to weakening of magnetization,[19] and lattice contraction. A contraction of 5−6% in the lattice parameter would give magnetization values in good agreement with the experimentally obtained values here. The actual contraction should be less due to surface effects and a finite temperature.

The calculated lattice parameter for bulk Fe_3S_4 spinel is 9.46 Å, compared to an experimental value of 9.876 Å.[22] This is larger than Fe_3O_4, where a = 8.43 Å; the agreement with experiment is also poorer, in part due to a very flat energy profile around the minimum. At the calculated energy minimum, the magnetization of the Fe_3S_4 spinel is 43 emu g^{-1}, which corresponds well with the experimental value for the bulk of 38 emu g^{-1}.[20] The magnetization would be higher at the experimental lattice parameter, according to GGA-PW91; however, we consider it more appropriate to take ground-state values for comparison with experiment.

LDA calculations performed for comparison found a value of 39 emu g^{-1} at the same value of a = 9.46 Å, consistent with the GGA-PW91 values. These values may be compared with the magnetization values measured in Table 1. The more than 3-fold reduction of magnetization from a calculated 43 emu g^{-1} in the bulk to an observed 12 emu g^{-1} at 10 K for nanocrystalline Fe_3S_4 is larger than the 2-fold reduction observed for Fe_3O_4. This indicates that size-related effects,[23] such as lattice contraction and surface magnetic effects play a more significant role for Fe_3S_4 than Fe_3O_4. This may be related to the relatively larger Fe−Fe distance in Fe_3S_4, because of the larger lattice parameter (more than 1 Å larger than Fe_3O_4).

T_B for 6 nm Fe_3S_4 and Fe_3O_4 nanocrystals is 50 and 100 K, respectively. Given the almost identical size distributions of the nanocrystals, the difference in T_B originates in a difference in magnetic anisotropy energy. Magnetic anisotropy energy can have contributions from shape and/or magnetocrystalline anisotropy.[24] The effective anisotropy of an ensemble of magnetic nanocrystals, K_{eff}, can be estimated from $K_{eff} = 25k_BT_B/\langle V\rangle$,[25] where k_B is the Boltzmann constant and $\langle V\rangle$ is the average particle volume. Assuming spherical geometries for the nanocrystals and substituting the average radii, K_{eff} values of 16 and −38.5 kJ m^{-3} for Fe_3S_4 and Fe_3O_4, are obtained, respectively. The sign of K_{eff} indicates the orientation of the easy axes of the phase: both Fe_3S_4 and Fe_3O_4 display cubic anisotropy, however the easy axes of Fe_3S_4 lie along the ⟨100⟩ directions,[24] and for Fe_3O_4 lie along the ⟨111⟩ directions.[26] The values obtained may be compared to values from the literature for the bulk phases. The first-order magnetocrystalline anisotropy constant, K_1, for Fe_3O_4 has been established as −20 kJ m^{-3} at 4 K,[26] but to the best of our knowledge K_1 has only ever been estimated for Fe_3S_4 ($K_1 \approx 1$ kJ m^{-3}) and this estimate did not appear to be based on experimental data.[27] The deviation of K_{eff} from K_1 for Fe_3O_4 (−20 cf. −38.5 kJ m^{-3}) indicates a strong shape anisotropy contribution to the thermal blocking behavior of the Fe_3O_4 nanocrystals. As both sets of nanocrystals have identical morphologies, it can be expected that shape anisotropy contributes a similar proportion to the effective anisotropy of the Fe_3S_4 nanocrystals. This leads to an estimated magnetocrystalline anisotropy constant of 8 kJ m^{-3} for Fe_3S_4.

In conclusion, monodisperse 6 nm Fe_3S_4 spinel nanocrystals have been synthesized by a new sulfidization method, a modification of which enabled the synthesis of isostructural Fe_3O_4 nanocrystals of identical average size. The temperature- and field-dependent magnetic properties of both sets of nanocrystals showed that the Fe_3S_4 nanocrystals had a saturation magnetization of 12 and 9 emu g^{-1} at 10 and 300 K, respectively, which is a more than 3-fold reduction compared to the calculated bulk value (43 emu g^{-1}). The blocking temperature of the Fe_3S_4 nanocrystals was lower than that of the Fe_3O_4 nanocrystals (50 and 100 K, respectively) and led to an estimate of 8 kJ m^{-3} for the magnetocrystalline anisotropy of the Fe_3S_4 spinel phase.

■ ASSOCIATED CONTENT

Supporting Information. Details of size selective purification and magnetic measurements. SAED, XRD patterns, and EDS analysis of the Fe_3S_4 and Fe_3O_4 nanocrystals and plot of variation in magnetic moments with lattice parameter. This material is available free of charge via the Internet at http://pubs.acs.org.

■ AUTHOR INFORMATION

Corresponding Author
*E-mail: richard.tilley@vuw.ac.nz.

■ ACKNOWLEDGMENT

The authors thank the MacDiarmid Institute of Advanced Materials and Nanotechnology for funding. R.D.T. thanks the Foundation for Science, Research and Technology for funding through Grant PROJ-13733-NMTS.

■ REFERENCES

(1) Wang, H.; Salveson, I. *Phase Transitions* **2005**, *78*, 547–567.
(2) Rickard, D.; Luther, G. W. I. *Chem. Rev.* **2007**, *107*, 514–562.
(3) Pósfai, M.; Kasama, T.; Chong, R. K. K.; Finlaysin, A. P.; Buseck, P. R.; Frankel, R. B.; Dunin-Borkowski, R. E. *Am. Mineral.* **2006**, *91*, 1216–1229.
(4) Dekkers, M. J.; Passier, H. F.; Schoonen, M. A. A. *Geophys. J. Int.* **2000**, *141*, 809–819.
(5) Roberts, A. P. *Earth. Planet. Sci. Lett.* **1995**, *134*, 227–236.
(6) Cheong, S.; Ferguson, P.; Feindel, K. W.; Hermans, I. F.; Callaghan, P. T.; Meyer, C.; Slocombe, A.; Su, C.-H.; Cheng, F.-Y.; Yeh, C.-S.; Ingham, B.; Toney, M. F.; Tilley, R. D. *Angew. Chem., Int. Ed.* **2011**, DOI:10.1002/anie.201100562.
(7) Takami, S.; Sato, T.; Mousavand, T.; Ohara, S.; Umetsu, M.; Adschiri, T. *Mater. Lett.* **2007**, *61*, 4769–4772.
(8) Liu, Z.; Zhang, D.; Han, S.; Li, C.; Lei, B.; Lu, W.; Fang, J.; Zhou, C. *J. Am. Chem. Soc.* **2005**, *127*, 6–7.

(9) Chen, X.; Zhang, X.; Wan, J.; Wang, Z.; Qian, Y. *Chem. Phys. Lett.* **2005**, *403*, 396–399.
(10) He, Z.; Yu, S.-H.; Zhou, X.; Li, X.; Qu, J. *Adv. Funct. Mater.* **2006**, *16*, 1105–1111.
(11) Vanitha, P. V.; O'Brien, P. *J. Am. Chem. Soc.* **2008**, *130*, 17256–17257.
(12) Beal, J. H. L.; Etchegoin, P. G.; Tilley, R. D. *J. Phys. Chem. C* **2010**, *114*, 3817–3821.
(13) Knobel, M.; Nunes, W. C.; Winnischofer, H.; Rocha, T. C. R.; Socolovsky, L. M.; Mayorga, C. L.; Zanchet, D. *J. Non-Cryst. Solids* **2007**, *353*, 743–747.
(14) Ma, J.; Chang, L.; Lian, J.; Huang, Z.; Duan, X.; Liu, X.; Peng, P.; Kim, T.; Liu, Z.; Zheng, W. *Chem. Commun.* **2010**, *46*, 5006–5008.
(15) Kresse, G.; Joubert, D. *Phys. Rev. B* **1999**, *59*, 1758–1775.
(16) Perdew, J. P.; Wang, Y. *Phys. Rev. B* **1992**, *45*, 13244–13249.
(17) Kresse, G.; Furthmüller, J. *Comput. Mater. Sci.* **1996**, *6*, 15–50.
(18) Perdew, J. P.; Zunger, A. *Phys. Rev. B* **1981**, *23*, 5048–5079.
(19) Fonin, M.; Pentcheva, R.; Dedkov, Y. S.; Sperlich, M.; Vyalikh, D. V.; Scheffler, M.; Rudiger, U.; Guntherodt, G. *Phys. Rev. B: Condens. Matter* **2005**, *72*, 104436–1−8.
(20) Tago, T.; Hatsuta, T.; Miyajima, K.; Kishida, M.; Tashiro, S.; Wakabayashi, K. *J. Am. Ceram. Soc.* **2002**, *85*, 2188–2194.
(21) Spender, M. R.; Coey, J. M. D.; Morrish, A. H. *Can. J. Phys.* **1972**, *50*, 2313–2326.
(22) Skinner, B. J.; Erd, R. C.; Grimaldi, F. S. *Am. Mineral.* **1964**, *49*, 543–555.
(23) Li, Z.; Sun, Q.; Gao, M. *Angew. Chem., Int. Ed.* **2005**, *44*, 123–126.
(24) O'Handley, R. *Modern Magnetic Material: Principles and Applications*; John Wiley & Sons: New York, 2000.
(25) Tackett, R.; Sudakar, C.; Naik, R.; Lawes, G.; Rablau, C.; Vaishnava, P. P. *J. Magn. Magn. Mater.* **2008**, *320*, 2755–2759.
(26) O'Handley, R. C. *Modern Magnetic Materials: Principles and Applications*; John Wiley and Sons: New York, 2000.
(27) Ricci, J. C. D.; Kirschvink, J. L. *J. Geophys. Res.* **1992**, *97*, 17 309–17 315.